Method of calibration of a fluorescence microscope for quantitative studies

K A T A R Z Y N A   M.   K E D Z I O R A †,   J O H E N   H.M.   P R E H N *,
J U R E K   D O B R U C K I †   &   T Y T U S   B E R N A S *·†

Department of Physiology and Medical Physics and RCSI Neuroscience Research Centre, Royal College of Surgeons in Ireland, Dublin, Ireland

†*Department of Biochemistry, Biophysics and Biotechnology, Jagiellonian University, ul. Gronostajowa 7, Krakow, Poland*

Summary

Confocal microscopy is based on measurement of intensity of fluorescence originating from a limited volume in the imaged specimen. The intensity is quantized in absolute (albeit arbitrary) units, producing a digital 3D micrograph. Thus, one may obtain quantitative information on local concentration of biomolecules in cells and tissues. This approach requires estimation of precision of light measurement (limited by noise) and conversion of the digital intensity units to absolute values of concentration (or number) of molecules of interest. To meet the first prerequisite we propose a technique for measurement of signal and noise. This method involves registration of a time series of images of any stationary microscope specimen. The analysis is a multistep process, which separates monotonic, periodic and random components of pixel intensity change. This approach permits simultaneous determination of dark and photonic components of noise. Consequently, confidence interval (total noise estimation) is obtained for every level of signal. The algorithm can also be applied to detect mechanical instability of a microscope and instability of illumination source. The presented technique is combined with a simple intensity standard to provide conversion of relative intensity units into their absolute counterparts (the second prerequisite of quantitative imaging). Moreover, photobleaching kinetics of the standard is used to estimate the power of light delivered to a microscope specimen. Thus, the proposed method provides in one step an absolute intensity calibration, estimate of precision and sensitivity of a microscope system.

Introduction

Confocal microscopy is a routine technique of imaging cells and tissues in three dimensions. This form of microscopy generates series of optical sections by moving focal volume with respect to a specimen. Pixel (voxel) of a confocal micrograph represents fluorescence signal integrated over a limited 3D PSF of a microscope (Brakenhoff *et al.*, 2005; Zwier *et al.*, 2008). The signal is quantized in absolute (albeit arbitrary) units. Thus, one may obtain quantitative information on local concentration of biomolecules in imaged material with this technique (Andrews *et al.*, 2002; Huang & Murphy, 2004; Fricker *et al.*, 2006). However, practical implementation of quantitative microscopy requires two elements. First, one has to convert fluorescence intensity to absolute units (for example, a number of molecules of interest). This task can be realized using an independent technique to provide a calibration curve (Model & Blank, 2006; Sugiyama *et al.*, 2005; Young *et al.*, 2006; Zwier *et al.*, 2008). The calibration depends on the detection volume (3D PSF), which is determined by the numerical aperture of the objective lens, the size of confocal pinhole and the wavelengths of emission and excitation (Wilson 1995; Zwier *et al.*, 2008). Moreover, the power of excitation light has to be measured independently in order to normalize fluorescence intensity in such calibration.

Second, one has to account for the limited precision of fluorescence intensity estimation (measurement error) which affects the final results of image analysis (Nicholson, 1978; Young, 1996; Stelzer, 1998; Zwier *et al.*, 2004; Vermolen *et al.*, 2005). Sources of this uncertainty may include instability of the light source, optical aberrations, and imperfections in alignment of elements in the optical path (Zucker, 2006a, b). Even when these problems are minimized, the presence of detector noise limits precision of quantitative microscopy (Jericevic *et al.*, 1989; Young, 1996; van den Doel *et al.*, 1998). The measurement noise may be estimated using a standard slide made with uniformly fluorescent beads (Zucker & Price, 2001a, b) or a piece of fluorescent plastic (van den Doel *et al.*, 1998; Mullikin *et al.*, 1994). Using this approach, one may measure only the total photonic noise

Correspondence to: Tytus Bernas, Department of Physiology and Medical Physics, RCSI, 123 St. Stephens Green, Dublin 2, Ireland. Tel.: +343-1-402-8518; fax: +353-1-402-8639; e-mail: tytusbernas@rcsi.ie

corresponding to a single level of intensity (the dark noise must be estimated separately). Moreover, comparison of signal-to-noise ratio between different microscope systems (or sets measurement conditions) requires separate determination of fluorescence excitation power. Finally, results obtained using such a standard sample may not be easily extended to the conditions under which actual biological specimens are imaged.

To rectify these problems we introduce a simple microscope specimen for confocal imaging to measure simultaneously several levels of fluorescence intensity. Variations of the intensity in time-lapse imaging are characterized using data-driven modeling to estimate the signal and its variance. We adapt the photon-transfer technique (Janesick *et al.*, 1987; Janesick, 1997; Howard, 2002) to describe magnitudes of the dark and photonic noise as a function of their respective signals (registered with a PMT). Similar approach was applied before in wide-field microscopy using a biological sample and a CCD detector (Bernas *et al.*, 2007). We take advantage of the fact that confocal detection volume is limited and extend that method by using a standard sample and providing an absolute calibration of fluorescence intensity (in molecules of equivalent soluble fluorophore, MESF). Thus the standard may be applied to compare intensities registered using different confocal microscopes or to ascertain reproducibility of measurements performed using the same system. Moreover, we demonstrate that the amount of excitation energy delivered to the sample can be determined from photobleaching kinetics of the standard. Thus, sensitivity of two microscope systems may be compared in absolute terms within the presented framework.

Materials and methods

Manufacturing of the standard

Polyvinyl alcohol (PVA, Mw 13 000–23 000, Sigma, Poland) was dissolved from solid in distilled and deionized water at the concentration of 6% w/w and mixed with a shaker for 6 h in 90°C. Stock solution of laser grade fluorescein was prepared by dissolving the dye in ethanol to the final concentration of 112.5 μM (verified spectrophotometrically). The stock fluorescein solution (1 μL) was mixed with the PVA solution (1 mL) with a vortex for 3 min (the final concentration of fluorescein in liquid PVA was 53 nM). The solution was prepared fresh before placing of 25 μL of PVA with fluorescein on a microscope coverslip (diameter 25 nm, thickness 0.17 mm). Coverslips were cleaned beforehand first with ethanol. The drop of PVA was left to dry for 24 h at 37°C. The coverslip was then mounted on a glass microscope slide with graphite rods (diameter 0.5 mm) used as spacers.

Microscope imaging. Image registration was performed using Leica SP5 confocal system based on DMI6000 microscope and equipped with Ar ion laser (Coherent, USA), acousto-optical beam-splitter (AOBS), a dry PlanApo CS 20x objective (NA = 0.7) and a 63x PlanApo CS oil immersion objective (NA = 1.4). The fluorescein fluorescence was excited with 488 nm light and collected in 495–535 and 545–620 nm wavelength ranges. Excitation power was adjusted using the AOBS between 1% and 20% of maximum laser output (1860 μW at the specimen). Time-lapse series of optical sections (512 × 512 pixels) were collected in a field of view containing a fluorescent region (PVA with fluorescein) and a region devoid of fluorescence (glass without polymer). The pixel dwell time ranged from 1.95 to 6.51 μs. A typical series comprised 500 frames registered every 0.32 s at the zoom of 1 for the 63× objective (3.1 for the 20× objective). The series were registered at 3 μm from the air–glass interface (as measured using reflected light). Where indicated series of optical sections through the standard or reference fluorescein solution were registered with 500 nm step. The corresponding voxel (pixel) size was 480 nm in the lateral (*xy*) direction, whereas the size in the axial direction (optical section thickness) corresponded to 970 nm (63×) and 1600 nm (20×), at the pinhole of 1.0 airy units.

Calculation of dark signal and noise levels and background signal. To estimate the background signal, uniform dark image regions were identified for each time series using method described previously (Bernas *et al.*, 2007). These regions (represented using binary masks) comprised pixels characterized by fluorescence intensity and local fluorescence heterogeneity that were smaller than 20% and 50% of their respective maxima. The initial masks were subjected to morphological closing an then to median filtering (using a kernel of 5 × 5 pixels for each operation) to exclude possible artefacts. Average intensity (I_b) calculated in dim and homogenous regions was taken as an estimate of the dark signal whereas the variance of I_b as an estimate of the dark noise, respectively. The initial background masks were subjected to dilation (circular kernel of 130 pixels in diameter), filing and erosion (kernel of 100 pixels in diameter) to eliminate regions containing little or no fluorescence signal from further calculations.

Decomposition of pixel intensity changes. The fluorescence signal measured in our system exhibits some spatial and temporal nonuniformity. Consequently, it is not possible to approximate a photon-transfer curve using standard techniques, which require a completely uniform and stable fluorescent area. Therefore, spatial and temporal decomposition of the dataset regions which, contain fluorescence signal (i.e. were not excluded in the previous step) was performed. First, the time series of pixel intensity values were divided by their respective averages:

$$I_{\text{NORM}}^i = \frac{I^i}{I_{\text{AVG}}^i}, \tag{1}$$

where I^i is the vector (T time points) of the intensities measured at ith pixel and I^i_{AVG} is the average of I^i taken over the T points. The normalized series (vectors) were grouped using k-means algorithm into three clusters, using city-block metrics as the similarity measure so as to minimize within-cluster sum of vector-to-centroid distances:

$$\arg\min_S \sum_{k=1}^{3} \sum_{I^i_{NORM} \in S_k} \| I^i_{NORM} - C_k \|, \qquad (2)$$

where $S_k \in \{S_1, S_2, S_3\}$ are clusters (partitions) of intensity vectors, C_k is the centroid of kth cluster and $\|\ \|$ is the sum (taken over T time points) of absolute differences between ith intensity vector and centroid of the respective cluster. The partitioning was repeated five times with the initial positions of cluster centroids chosen randomly. The partition which corresponds to the smallest sum of distances from each vector to its cluster centroid was selected. The centroids which corresponded to clusters of less than 5000 vectors were discarded. If there were still three centroids in the resulting set then the two of them (which were the most dissimilar, as measured with city-block metrics) were chosen for further analysis. Otherwise all centroids were retained as signal templates. A weighted sum of two centroids (or one centroid) was fitted to each of vectors using the weights as the fitting parameters:

$$S^i = w^i_1 C_1 + w^i_2 C_2, \qquad (3)$$

where S^i is the time vector of estimated signal intensity, w^i are scalar weights corresponding to the ith pixel intensity vector. The operation was executed using nonlinear least squares approach with Levenberg–Marquardt algorithm:

$$\arg\min_{w^i_1, w^i_2} \sum_{t=1}^{T} [S^i_t(w^i_1, w^i_2) - I^i_t]^2, \qquad (4)$$

where I^i_t are the elements of vector I^i (eq. 1) and S^i_t are the elements of vector S^i (Eq. 3). The weights were constrained between minimum and maximum possible image intensity. The fitted sums of centroids represents the true instantaneous fluorescence intensity (signal, S^i_t) at every time point. Hence, the instrumental noise (for a pixel at a given time point) and its variance (for a signal level) was (Bernas *et al.*, 2007):

$$N^i_t = \left| S^i_t - I^i_t \right|, \quad V_{S=F} = \frac{\sum\limits_{i,t} \delta_{SF}(N^i_t)^2}{\sum\limits_{i,t} \delta_{SF}}, \qquad (5)$$

where N is the noise, S is the signal, I is registered fluorescence intensity at ith (pixel) and tth (time) points of the image time series, $V_{S=F}$ is variance of the signal at Fth level.

Noise model. To characterize the dependence between signal and noise we adopted the approach presented in (Janesick *et al.*, 1997) where the noise was composed of several independent sources:

$$\sigma_T^2 = \sigma_P^2 + \sigma_D^2 + \sigma_L^2, \qquad (6)$$

where the variances (given as the respective squared standard deviations) correspond to: the total noise (σ_T), the photonic (shot) noise (σ_P), the dark current noise (σ_D) and a current-independent (readout) noise (σ_L). The latter component is due to the presence of preamplifier (operated at fixed factory settings), the load resistance and ohmic leakage (Pawley, 1994; Enstrom, 1989). Because the photonic and dark current noise are produced by secondary electrons their magnitudes were determined by Poisson statistics and equal to the respective signals (measured in electrons):

$$\sigma_P^2 = S_P^e(t, p, e), \ \sigma_D^2 = S_D^e(t). \qquad (7)$$

In confocal scanning microscopy the photonic signal (S_p^e) is a function of pixel dwell time (t), optical section thickness (p) and excitation power (e). The dark signal (S_d^e) depends only on the first of these parameters. The number of arbitrary digital units (ADU) output by a confocal detector (photomultiplier, PMT) is related to the number of electrons by the PMT gain. Therefore,

$$\begin{aligned} V_P^{ADU} &= G_{ADU/e}^2 \times S_P^e = G_{ADU/e} \times S_P^{ADU}, \\ V_D^{ADU} &= G_{ADU/e}^2 \times S_D^e = G_{ADU/e} \times S_D^{ADU}, \end{aligned} \qquad (8)$$

where $G_{ADU/e}$ is the conversion factor (gain) corresponding to of ADU output for one electron, S correspond the signal levels and V to their respective variances (photonic and dark), measured in ADU. One should note that $G_{ADU/e}$ contains also multiplicative noise (Pawley, 1994). The noise model described in Eq. (2) may be thus represented in digital units:

$$V_T^{ADU} = G_{ADU/e} \times S_P^{ADU} + G_{ADU/e} \times S_D^{ADU} + C_L, \quad (9)$$

where V_T^{ADU} the total variance and C_L the readout noise (measured in ADU). Following the previous work (Bernas *et al.*, 2007) total noise variance (V, an estimator of V_T^{ADU} calculated using Eq. 1) was plotted against the signal corrected for background ($S_c = S - I_b$, estimator of S_P^{ADU}). A linear function was fitted to these data to characterize signal-to-noise dependency:

$$V = A + P S_c, \qquad (10)$$

where P, and A are estimators of the signal variance associated with the photonic (Poisson), and the additive noise components. The former corresponds to gain ($G_{ADU/e}$) whereas the latter to the sum of variances due to the dark and readout noise components ($V_D^{ADU} + C_L$). One should note that quadratic term used previously in (Bernas *et al.*, 2007) did not improve the fit significantly (as discussed further) and was omitted here.

Photobleaching kinetics. The decrease of fluorescence of the standard imaged using different power of excitation light was used to characterize photobleaching (Bernas *et al.*, 2004). Briefly, signal estimates (S^i_t) were constructed for every nonbackground time series of pixel values and sum of two exponential functions is fitted to the estimates.
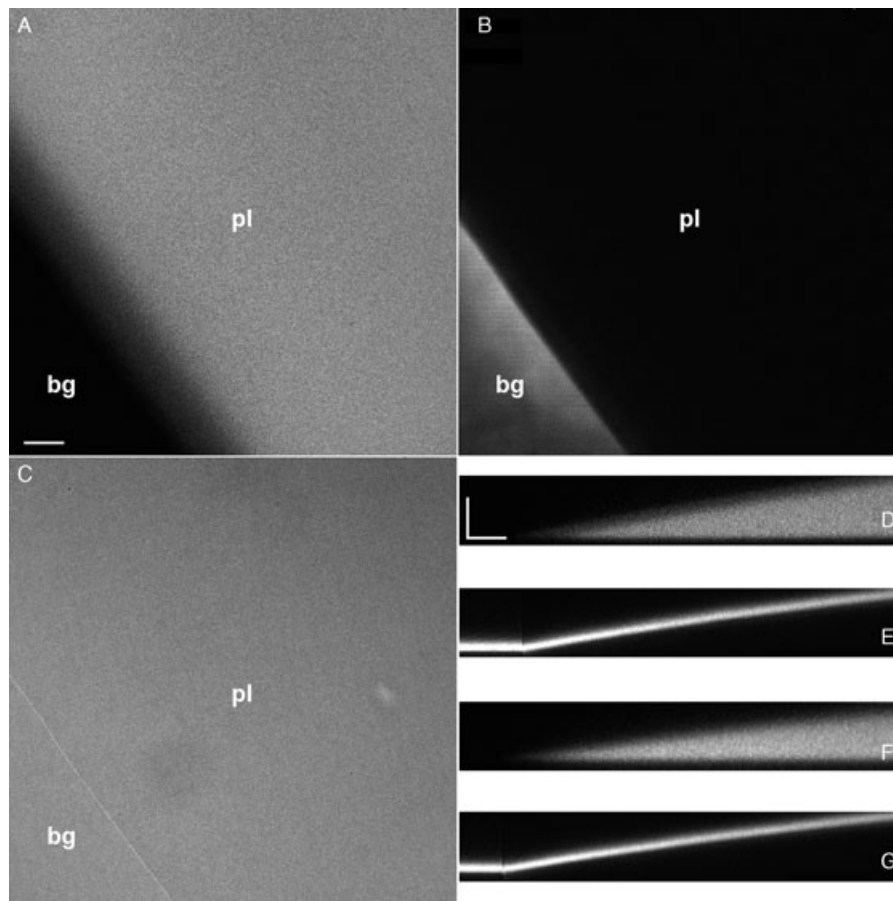
Fig. 1. Horizontal (*xy*) optical section through the standard imaged using fluorescence (A), transmitted light (B) and backscattered light (C). Vertical (*xz*) cross section through polymer and coverslip (fluorescence, DF and reflected light, EG) of the standard. The images were registered with oil immersion objective (63×, NA 1.4, panels A–C, D and F) and air objective (20×, NA 0.45, panels F and G). Gradient of intensity in the region containing polymer (pl) is clearly separated from the uniform background (bg). Scale bars 10 μm (*x* direction) and 5 μm (*z* direction), respectively.

The rates of photobleaching were calculated on pixel-by-pixel basis as the first order derivatives of these functions, taken at 0 time (Bernas *et al.*, 2004). The pixel rates were divided by the respective series average values and the overall photobleaching rate of the standard was calculated as the median of the distribution of the normalized values corresponding to pixel series.

Intensity calibration. A series of solutions of fluorescein (concentrations ranging from 0.435 to 4.35 μM) was prepared in PBS (pH = 11). Optical sections are registered through the solutions with the gain from 400 to 800 V, pixel dwell time 3.9 μs and the pinhole set from 1.0 to 2.5 Airy units. Functional relationship between average fluorescence intensity and the fluorescein concentration is established using linear regression ($r^2 > 0.94$). Images of the standard were registered using the same settings and equivalent concentration of fluorescein molecules was calculated using average intensity in the filled optical section of the standard as the input. This equivalent

concentration was used to calculate the number of molecules of equivalent soluble fluorophore (MESF) corresponding to a voxel. The detection volume (3D PSF) was estimated using theoretical lateral (*xy*) dimensions (Wilson, 1995) and axial (*z*) dimension measured with a series of optical sections through the standard. The MESF value was correlated with the fluorescence intensity of the standard normalized with respect to the excitation energy density. It may be noted that the calibration thus incorporated possible differences of quantum efficiencies of the fluorophore in solution on the solid support.

Results

Characteristics of the standard

The standard contains a region occupied by the fluorescent polymer and a region devoid of the polymer and therefore nonfluorescent (Fig. 1A). The interface between glass and polymer reflects little light in comparison with the interface between glass and air (Fig. 1B, E and G). Neither of the regions
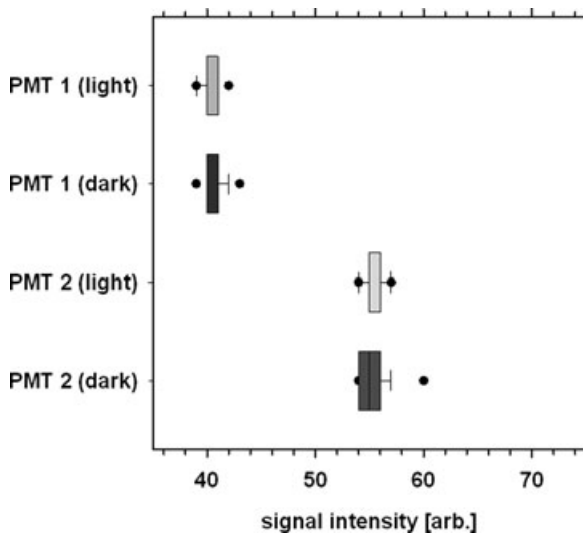
Fig. 2. Distribution of intensity in the background region in the absence (dark) and the presence of illumination (light). The intensity was measured using in the 495–535 nm (PMT 1) and 545–620 nm (PMT2) wavelength ranges. The boxes represent medians, 25 and 75 percentiles, the whiskers correspond to 10 and 90 percentiles, whereas the whiskers 5 and 95 percentiles of the distribution.

absorbs light significantly (Fig. 1C). Owing to the curvature of the polymer drop several levels of fluorescence intensity are represented in the image (Fig. 1A and D). This notion holds both for oil (Fig. 1D and E) and air (Fig. 1F and G) used as the immersion medium. Within that region areas of maximum signal correspond to complete fill of optical sections by the polymer (Fig. 1A, D and F and 2), whereas in the areas of intermediate intensity correspond to partial fill. By contrast, the nonfluorescent region contains instrumental background signal and corresponding noise (Figs. 1A and 2). As expected, this background intensity distribution in this region is not affected by illumination, as estimated using two independent detectors (Fig. 2).

The presence of several levels of fluorescence intensity in one field of view makes it possible to calculate complete signal to noise characteristics (as described further). It should be noted that the maximum intensity is similar in different parts of the standard, as demonstrated by the vertical (xz) intensity profiles (Fig. 3). The reproducibility me manufacturing estimated in this way corresponds to 95% similarity between standards (data not shown). The maximum intensity decreases slightly with the depth in the standard (Fig. 3), owing to scattering of light. Thus, images are registered in further experiments at the same distance from the coverslip (as described in Section "Materials and Methods").

Determination of signal and noise

Following registration of time lapse series of images of the standard the magnitudes of signal and noise levels are analysed on pixel-by-pixel basis. The noise variance increases with the signal as shown using the photon transfer curve (Fig. 4). The fact that the dependence may be adequately characterized with a linear function that the detector (photomultiplier) operated mostly in linear range. A significant deviation from linearity is observed at only the highest values of the signal (discussed further). The directional coefficient (P) of this function is a measure of the level of signal (photonic) noise, whereas the constant (A) corresponds to the magnitude of dark noise.

As expected, photonic noise increases with decreasing pixel dwell time (Fig. 5A, Table 1). It should be noted that increase of the time by two to reduces the respective noise (variance) coefficient by approximately the same factor (Table 1). By contrast, the time does not affect the average signal magnitude (image intensity). The signal increases with detector gain, though. One should note that linear increase of gain (PMT voltage) results in corresponding exponential increase of photonic noise (Fig. 5A, Table 1). Similarly, the magnitude of dark noise (estimated from the photon transfer curve) increases with gain but decreases with pixel dwell time (Fig. 5B, Table 1). This notion is supported by the estimate of dark noise and signal from image background (Table 1). These two estimates are similar at low and moderate gain. However, at the high gain the estimate obtained from the photon transfer curve was higher compared to its counterpart from the image background. By contrast, product of the directional coefficient (P) and the dark signal coincides with the estimate obtained by extrapolation of the curve to zero signal (Table 1). This notion indicates that the noise calculated from the image background may be underestimated. It should be noted that both forms of noise were independent of the detector offset (data not shown).

Linear fit (Eq. 10) of the photon transfer model was compared with the quadratic one (Bernas *et al.*, 2007). However, the respective linear and constant coefficients were equal (within one standard deviation) and the quadratic coefficients were equal to 0 (data not shown, but available to the reviewers). Thus, the linear model (Eq. 10) was sufficient to explain the data. One may postulate that this simple model would perform adequately for any light detector (including PMTs) with similar characteristics of signal and noise.

Intensity calibration of the standard

The functional dependence between noise and signal is not affected by the choice of the units that the intensity is expressed in. However, the fluorescence signal may be correlated with the concentration of fluorescence molecules observed within a focal volume in solution (Fig. 6A). Fluorescence intensity registered in the solution increases with the confocal pinhole and the detector gain but does not depend on pixel dwell time. Thus, the latter parameter can be disregarded in the presented calculations but it may be necessary to include when different microscope system is calibrated. The fluorescence intensity of the standard (measured in the region corresponding to filled
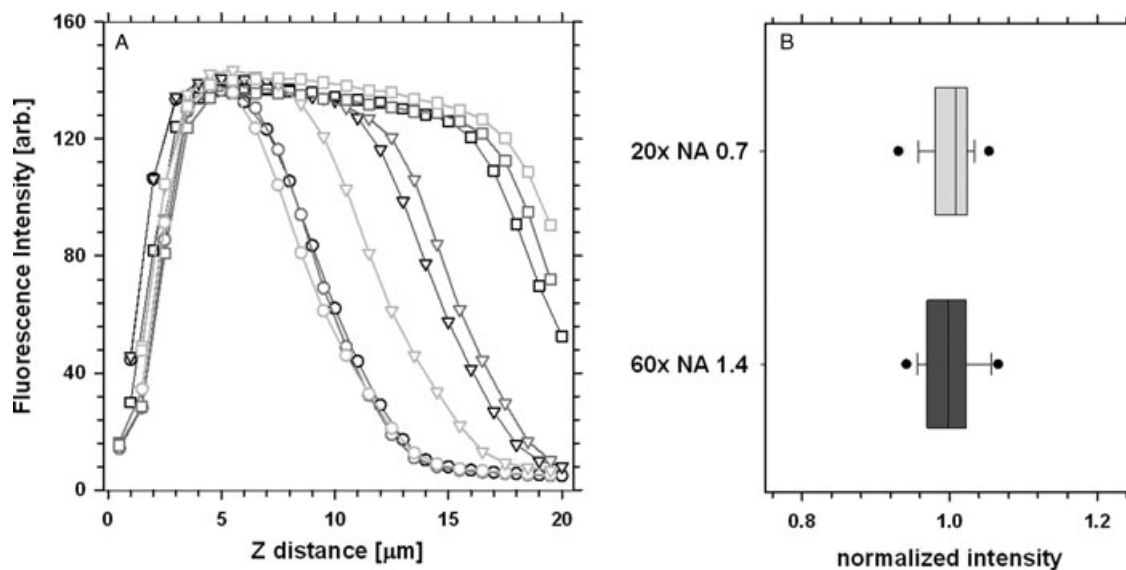
Fig. 3. Spatial uniformity of the standard. Fluorescence intensity profiles (panel A) corresponding to different fields of view in the standard (marked with circles, triangles and squares, respectively). The intensity was measured in several square regions of interest (marked with back, dark and light grey lines) in each field of view. Normalized fluorescence intensity distribution (panel B) corresponding to five fields of view in the standard, comprising 10 regions each. The intensity was registered with $20\times$ (light grey) and $60\times$ (dark grey) objectives. The boxes represent medians, 25 and 75 percentiles, the whiskers correspond to 10 and 90 percentiles, whereas the whiskers 5 and 95 percentiles of the distribution.

optical section) may be equated to that of a solution (Fig. 6A), provided that the respective sizes of detection volumes (determined in *z* direction by the size of confocal pinhole) are the same. In other words, the detected fluorescence intensity
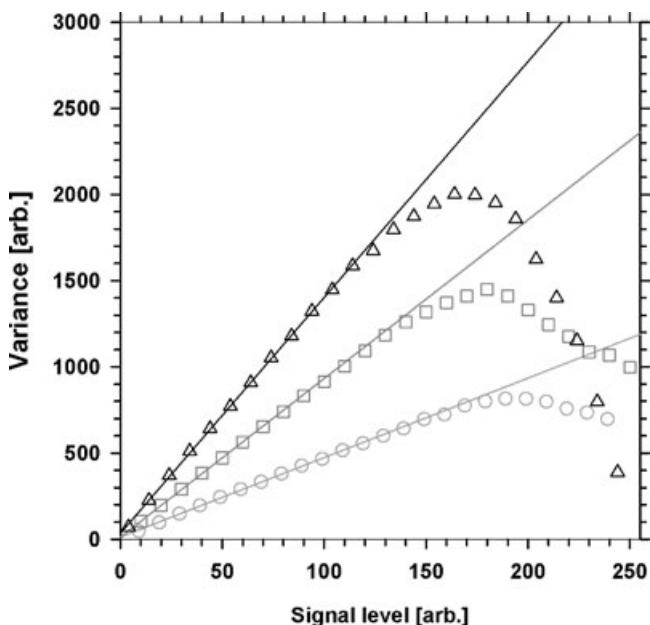

Fig. 4. Examples of photon transfer curves corresponding to the data registered at short (1.95 μs, triangles), intermediate (3.25 μs, squares) and long (6.51 μs, circles) pixel dwell time. The points represent the average variance corresponding to a given signal level (plotted every 10th level), whereas the lines represent fits to the linear curve fragments.

is affected similarly by the imaging conditions in the solution (known concentration of fluorophore molecules) and in the standard. Hence, the fluorescence of the latter (normalized with respect to the energy density of excitation light) can be expressed in terms of number of molecules of equivalent soluble fluorophore (MESF, Fig. 6B). This dependence may be described using equation:

$$N^{\mathrm{MESF}} = C \log_{10}\left(S^{\mathrm{ADU}}_{\mathrm{NORM}}\right) + D, \qquad (11)$$

where N^{MESF} is the number of molecules, $S^{\mathrm{ADU}}_{\mathrm{NORM}}$ is the normalized fluorescence intensity, C and D are fit coefficients. The respective numerical results are given in the Table 2. One may note that that these two coefficients are affected by detector gain but not other parameters of image registration. This equivalence should be understood in terms of the same detected fluorescence of both standard and solution, whereas the actual concentrations may not be identical (owing to differences in quantum efficiency).

Estimation of the excitation power with photobleaching

Repeated illumination of a region in the standard results in a loss of fluorescence intensity (Fig. 7A). The loss of intensity in the presented system is irreversible (data not shown). The kinetics of this photobleaching may be adequately represented using sum of two exponents (Fig. 7A). The initial photobleaching rate (calculated from first derivative of the fitted curve and normalized with respect to the average intensity) depends on the excitation power, pixel size and
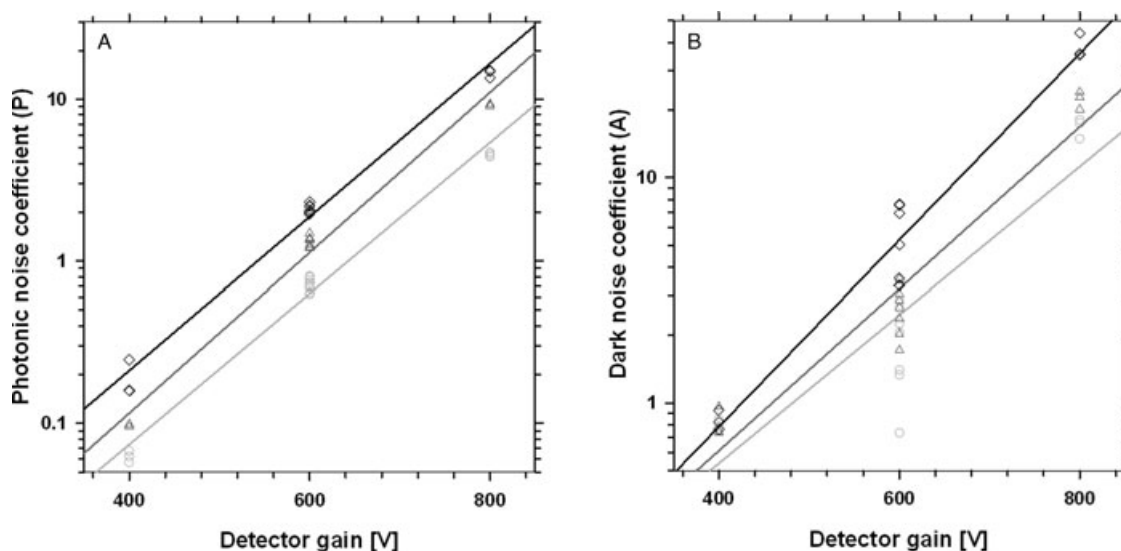
Fig. 5. Influence of image registration parameters on photonic (A) and dark (B) noise. The magnitudes of these two forms of noise were estimated with photon transfer curve (coefficients P and V, respectively). The data were registered with dwell times of 1.95 μs (diamonds), 3.25 μs (triangles) and 6.51 μs (circles). The lines represent to linear fits corresponding to these pixel dwell times (light grey, dark grey and black, respectively).

pixel dwell time but is not affected by detector gain. The rate increases monotonically with the amount of excitation light (its energy density) delivered during registration of a single image frame (Fig. 7B). This effect may be described using equation:

$$R_{\mathrm{NORM}} = TW^{U}, \qquad (12)$$

where R_{NORM} is the normalized photobleaching rate, W is the energy density of light, T (0.0154 ± 0.0015) and W (0.619 ± 0.016) are fit coefficients ($r^2 = 0.99$). Therefore, the rate may be used to estimate power delivered to a unit of area (detection volume within optical section) in the sample.

Discussion

Quantitative microscopy requires information on the precision and sensitivity of light detection. Comprehensive characteristics of detector performance can be obtained out of a microscope, using specialized test benches (Creusot *et al.*, 2002; Howard, 2002; Ajaltounia *et al.*, 2003; Christen *et al.*, 2005). The presented technique provides less detailed results but requires only a time series of images of a simple microscope specimen. Hence, it can be implemented in any lab without need for specialized equipment or disassembling the microscope. Estimation of the dependence between the noise and the signal is performed similarly to the photon-transfer curve approach (Janesick, 1997; Howard, 2002; Christen *et al.*, 2005; Kinney & Talbot, 2006). Input data for this algorithm are generated with a combination of clustering and least squares regression, used to determine instantaneous signal (and noise) on a pixel-by-pixel basis. This method requires no information on the position of a pixel within image or characterization of pixel neighbourhood (spatial fluorescence distribution). Hence, it eliminates the need for spatial (Howard, 2002; Janesick, 1997) and temporal uniformity of the signal (Howard, 2002; Kinney & Talbot, 2006) and populates the majority of signal levels in the photon-transfer curve. By contrast, our method of signal estimation is less precise than simpler spatial (Janesick, 1997; Howard, 2002) or temporal (Howard, 2002; Kinney & Talbot, 2006) average (under optimal conditions). Thus, a large number of measurements corresponding to a single signal level is necessary ($>50\,000$ in our system).

Determination of the background area is carried out separately from the photon-transfer curve calculation. This approach renders manual segmentation (Howard, 2002; Kinney & Talbot, 2006) unnecessary and provides the second measurement of the dark noise. These two estimates differ only at the highest gain where the corresponding variance (the photon transfer estimate) could be too large to measure reliably. By contrast this value coincides with the estimate calculated using the directional coefficient (P) of the photon transfer curve and the dark signal as the inputs. Thus, it may be postulated that the analogue detector offset was too low (even if no pixels of zero value were present in the dataset), thus creating truncated distribution intensity of the background. It should be noted that the additive noise estimated from the constant coefficient (A) increased with the gain, similarly to the photonic noise. Therefore, it is likely that the major part of this form of noise was produced by the dark current, whereas the contribution of ohmic leakage and load noise (Enstrom, 1989; Pawley, 1994) was negligible. Moreover, the fact that linear model of the photon transfer was sufficient to describe the data indicates that the detector operated in linear range

Table 1. Dependence of the magnitudes of noise (photonic and dark) and dark signal on conditions of image registration. The noise was estimated using photon transfer curve, whereas the dark signal from image background. The values are given with their standard errors.

Pixel dwell time (μs)	Detector gain (V)	Photonic noise coefficient (P)	Dark noise variance (A, est. from fit)	Dark noise magnitude (est. from image bg.)	Dark noise variance (est. from image bg.)
6.51	400	0.062 ± 0.005	−0.19 ± 0.03	1.000 ± 0.001	0.001 ± 0.001
6.51	600	0.721 ± 0.068	1.53 ± 0.98	1.832 ± 0.452	1.482 ± 1.526
6.51	800	4.550 ± 0.147	15.82 ± 1.70	2.088 ± 0.017	2.431 ± 1.359
3.25	400	0.097 ± 0.001	−0.18 ± 0.13	1.000 ± 0.001	0.001 ± 0.001
3.25	600	1.323 ± 0.010	1.59 ± 0.61	1.967 ± 0.800	1.254 ± 1.000
3.25	800	9.200 ± 0.155	28.49 ± 8.24	2.618 ± 0.107	5.705 ± 1.399
1.95	400	0.189 ± 0.051	−0.16 ± 0.08	1.387 ± 0.543	0.048 ± 0.001
1.95	600	2.056 ± 0.104	4.02 ± 2.06	2.239 ± 0.829	2.919 ± 0.087
1.95	800	14.492 ± 0.862	33.32 ± 10.00	2.737 ± 0.105	10.790 ± 1.530

and additional noise sources (e.g. afterpulsing, Pawley, 1994) did not bring a significant contribution.

A different method of decomposition of pixel intensity into signal and noise components using random walks combined with harmonic regression was presented before (Bernas *et al.*, 2007). It was used successfully for characterization of CCD performance in wide-field microscopy, where loss of fluorescence intensity (photobleaching) during imaging was low (<25% of the initial intensity). However, these algorithms did not perform robustly for confocal data where photobleaching reached 60%, as it was the case with the system described here. Therefore clustering combined with

nonlinear least squares fitting was used instead. One should note that the method (similarly to the one used previously) requires a stationary specimen to register image time series. Therefore, presence of axial (*z*) or lateral (*xy*) specimen drift might impair accuracy of the presented method as it might contribute to pixel intensity variation. In our experience total lateral displacement does not exceed the value reported in (Bernas *et al.*, 2007) and thus does not influence significantly results of the calculations.

The algorithm described here estimated instantaneous signal and noise independently for each pixel and required no information on the position of a pixel within image or
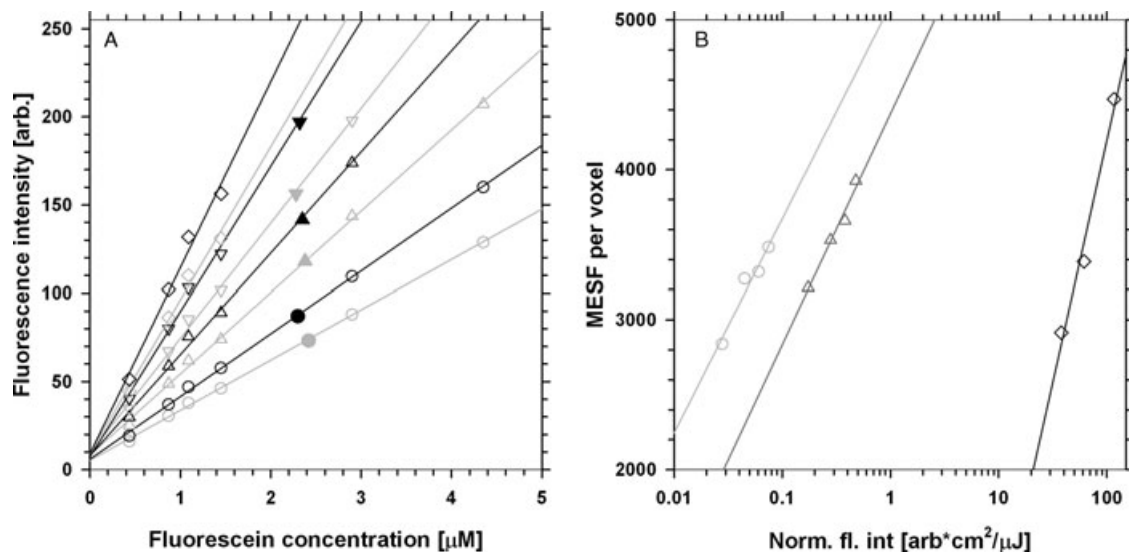

Fig. 6. Intensity calibration of the standard. Correlation of fluorescence intensity (*x* axis) with the concentration (*y* axis) of fluorescein molecules of fluoresce in solution (Panel A). The intensities were registered at the detector gain of 400 and 800 V (grey and black colour, respectively) and with pinhole sizes corresponding to 1.0, 1.5, 2.0 and 2.5 Airy units (open circles, triangles up, triangles down and diamonds, respectively). The lines represent to linear fits corresponding to these data. The closed symbols correspond to the standard registered in the same conditions as the fluorescein solutions (the intensity was measured, whereas the concentration predicted from the linear regression).Correlation of the normalized fluorescence intensity (Panel B) of the standard (*x* axis) with expected number of molecules of equivalent soluble fluorophore (MESF) a voxel (*y* axis). The intensities were registered at the detector gain of 400, 600 and 800 V (circles, triangles and diamonds, respectively). The lines (light, dark grey and black, respectively) represent the dependence between these two intensity parameters (Eq. 11, $r^2 > 0.95$). The respective fit coefficients are given in Table 2.

Table 2. The relationship between the number of molecules in solution (MESF) and the normalized signal intensity (Eq. 11). The respective fit coefficients (C, D) are given with their standard errors.

Detector gain (V)	Coefficient C	Coefficient D	Correlation (r^2)
400	1429 ± 248	5101 ± 328	0.97
600	1540 ± 172	4373 ± 93	0.98
800	2727 ± 664	-2257 ± 846	0.96

characterization of pixel neighbourhood. Therefore it may be used in connection with any nonuniform fluorescent microscope specimen (containing nonfluorescent regions). However, the fluorescence nonuniformity of the standard reflects varied degree of filing of the confocal section. Thus one may expect that the intensity corresponding to completely filled section is constant in given imaging conditions. A slight decrease of this value with the depth in the sample may be attributed to light scattering and accounted for when the imaging is performed at the same depth. One might include autofocusing routine in the algorithm to automate positioning. More importantly, some variability is detectable between standards and regions. The former is likely to result from casting process and is likely to be minimized with improvements in manufacturing and quality control (which is being implemented). The latter is caused by illumination nonuniformity, which can be eliminated with improvements in the microscope optics. Nonetheless, this factor can be accounted for if the calibration is performed separately for different regions in the microscope field of view. Alternatively, the image data can be corrected for this nonuniformity using another standard (SIP chart) as described in Brakenhoff *et al.* (2005) and Zwier *et al.*, (2006). Because the proposed standard can provide an uniformly fluorescent volume it seems feasible to adapt for the presented system the approach described by these authors.

The intensities of signal and noise can be expressed in absolute units of fluorophore concentration. The standard may be used quantitatively intensities registered using different confocal microscopes or to ascertain reproducibility of measurements performed using the same system. Similar techniques which rely on measurement of the total fluorescence within focal volume were presented by others (Model & Blank, 2006). A different approach to this problem was adopted in (Zwier *et al.*, 2004, 2008) where a uniformly thin layer of fluorescent material (SIP chart) is used to sample the focal spot (thus estimating average fluorescence). This method has the advantage of providing inherent correction for the nonuniformity of illumination (detection) efficiency over a field of view. However, using this type of standard one may readily estimate only the total noise corresponding to a single level of intensity (provided that a sufficiently uniform region in found in an image). It should be noted that all methods of standardization described here provide only absolute measure of detected fluorescence but not an estimate of a number (concentration) of fluorochrome molecules in a specimen imaged with a microscope system.

Kinetics of changes of fluorescence signal in time, estimated with the presented algorithm, may be used to characterize
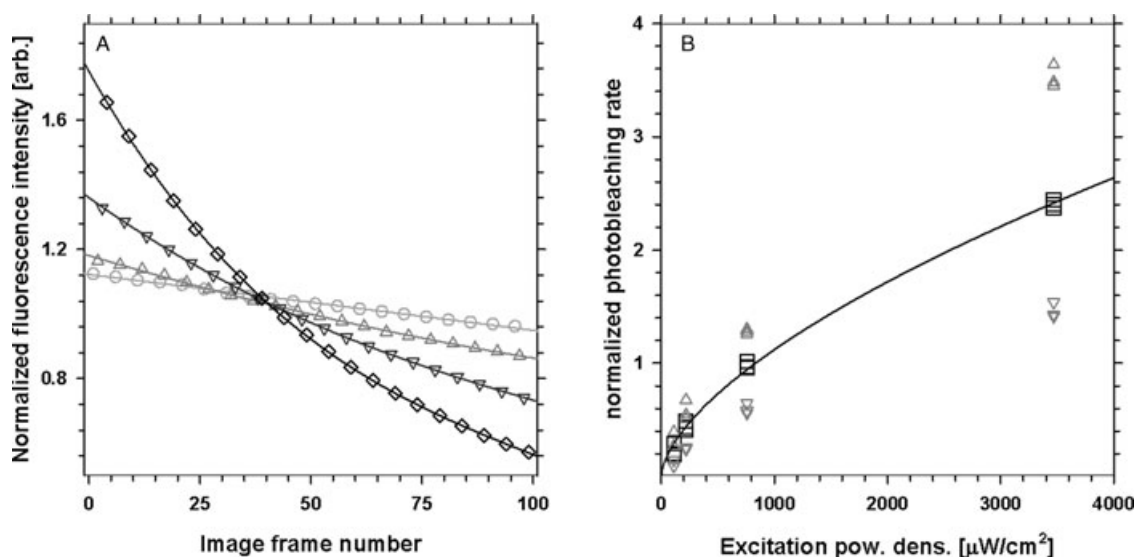

Fig. 7. Kinetics of photobleaching of the standard illuminated with 113 μW cm^{-2} (circles), 220 μW cm^{-2} (triangles up), 758 μW cm^{-2} (triangles down) and 3468 μW cm^{-2} (diamonds) density of excitation light, panel (A). The lines correspond to bi-exponential representations of the photobleaching curves. Correlation of the normalized photobleaching rates (*y*-axis) with the power density of excitation light (*x*-axis), panel (B). Squares represent the median rates (calculated over initial intensity levels), whereas triangles the 25 and 75 percentiles of rate distribution. The curve (black) corresponds to a power function fit (Eq. 12).

photobleaching. The magnitude of this fluorescence loss depends on the dose of light (Wilson *et al.*, 1997; Bernas *et al.*, 2004; Van Oostveldt *et al.*, 1998) and thus may be used to estimate this quantity. Similar dosimetric technique has been used in photodynamic therapy (Wilson *et al.*, 1997; Dysart *et al.*, 2005; Mphil *et al.*, 2005). This implicit dosimetry is a simple approach capable of measuring the dose delivered to the sample, as opposed to the explicit method, which requires an external meter (Wilson *et al.*, 1997). However, the latter approach is more precise than the former. Likewise, the presented results are less precise than a measurement with properly configured power meter. However, the estimate is obtained using the same set of data as used for other analysis steps described here.

In conclusion, the methodological approach presented here provides signal-to-noise characteristics of the detector, absolute calibration of intensity, and an estimate of excitation dose (power) using one set of time-lapse images. Once established, these characteristics depend only on specifications of a microscope system and imaging conditions. Therefore, one may perform quantitative measurements of any specimens with a calibrated system. Moreover, it is possible to compare quantitatively images registered using different confocal microscopes or to ascertain reproducibility of measurements performed using the same system. The necessary data are collected using a standard microscope specimen, which is simple, inexpensive to manufacture and may potentially be used with other fluorophores.

Acknowledgements

References

Ajaltounia Z., Bohnera G., Carloganua C., Cornata R., Crouaua M. & Deschamps O. (2003) Study of Multianode Photomultipliers for the electromagnetic calorimeter preshower read out of the lhcb experiment. *Proceedings of the 3rd International Conference on New Developments in Photodetection*, Beaune, France June 17–21.

Andrews, P. D., Harper, I. S. & Swedlow, J. R. (2002) To 5D and beyond: quantitative fluorescence microscopy in the postgenomic era. *Traffic* **3**(1), 29–36.

Bernas, T., Asem, E.K., Robinson, J.P. & Rajwa, B. (2007) Precision of light intensity measurement in biological optical microscopy. *J. Microsc.* **226**(2): 163–174.

Bernas, T., Zarebski, M., Cook, P. R. & Dobrucki, J. W. (2004) Minimizing photobleaching during confocal microscopy of fluorescent probes bound to chromatin: role of anoxia and photon flux. *J. Microsc.* **215**, 281–296.

Brakenhoff, G.J., Wurpel, G.W., Jalink, K., Oomen, L., Brocks, L. & Zwier J.M. (2005) Characterization of sectioning fluorescence microscopy with thin uniform fluorescent layers: sectioned imaging property or SIP charts. *J Microsc.* **219**(3), 122–132.

Christen, F., Kuijken, K., Baade, D., Cavadore, C., Deiries, S. & Iwert, O. (2005) Fast conversion factor (gain) measurement of a CCD using images with vertical gradient. *Proceedings of the Scientific Devices Workshop*, Taormina, Italy.

Creusot, A., Genolini, B., Nguyen Trung, T. & Pouthas, J. (2002) *Comparison of Photonis and IPN-Orsay test benches used for the photonis XP 1805 PMT gain measurements*, GAP-2002-042, 1–6.

van Den Doel, L. R., Klein, A. D., Ellenberger, S. L., Netten, H., Boddeke, F. R., van Vliet, L. J. & Young, I. T. (1998) Quantitative evaluation of light microscopes based on image processing techniques. *Bioimaging* **6**, 138–149.

Dysart J. S., Singh G. & Patterson M. S. (2005) Calculation of singlet oxygen dose from photosensitizer fluorescence and photobleaching during mTHPC photodynamic therapy of MLL cells photochem. *Photobiol.* **81**(1), 196–205.

Engstrom, R. W. (1989) *Photomultiplier Handbook*, RCA/Burle, New York, U.S.A., pp. 36–80.

Fricker, M., Runions, J. & Moore, I. (2006) Quantitative fluorescence microscopy: from art to science. *Annu. Rev. Plant. Biol.* **57**, 79–107.

Howard, N. E. (2002) *Photon Transfer Technique*. Opsci Application Note OAN-006, OPSCI. (http:www.opsci.com).

Huang, K. & Murphy, R. F. (2004) From quantitative microscopy to automated image understanding. *J. Biomed. Opt.* **9**(5), 893–912.

Janesick, J. R. (1997) CCD transfer method: standard for absolute performance of CCDs and digital CCD camera systems. *Proc. SPIE.* **3019**, 70–102.

Janesick, J., Klaasen, K & Elliott, T. (1987) CCD charge collection efficiency and the photon transfer technique. *Opt. Eng.* **26**(10), 972–980.

Jericevic, Z., Wiese, B., Bryan, J. & Smith, L. C. (1989) Validation of an imaging system: steps to evaluate and validate a microscope imaging system for quantitative studies. *Methods Cell. Biol.* **30**, 47–83.

Kinney, P. D. & Talbot, R. J. (2006) Methods and systems for in situ calibration of imaging in biological analysis. Applera Corporation, 911.

Mphil M.A., Stringer M.R., Cruse-Sawyer J.E., Dyera P.E. & Brown S.B. (2005) The influence of intracellular mTHPC concentration upon photobleaching dynamics. *Photodiag. Photodyn. Ther.* **2**(3), 235–238.

Model M.A. & Blank J.L. (2006) Intensity calibration of a laser scanning confocal microscope based on concentrated dyes. *Anal Quant. Cytol. Histol.* **28**(5), 253–261.

Mullikin, J. C., van Vliet, L. J., Netten, H., Boddeke, F. R., Van Der Feltz, G. & Young, I. T. (1994) Methods for CCD camera characterization. *Proc. SPIE.* **2173**, 73–84.

Nicholson, W. L. (1978) Application of statistical methods in quantitative microscopy. *J. Microsc.* **113**(3), 223–239.

Pawley, J. (1994) Sources of noise in three-dimensional microscopical data sets. *Three-Dimensional Confocal Microscopy: Volume Investigation of Biological Specimens* (ed. by J. Stevens, L. Mills, J. Trogadis), pp. 47–94. Academic Press, San Diego, CA.

Stelzer, E. H. K. (1998) Contrast, resolution, pixelation, dynamic range and signal to noise ratio: fundamental limits to resolution in fluorescence light microscopy. *J. Microsc.* **189**(1), 15–24.

Sugiyama, Y., Kawabata, I., Sobue, K. & Okabe, S. (2005) Determination of absolute protein numbers in single synapses by a GFP-based calibration technique. *Nat. Methods* **2**(9), 677–684.

Van Oostveldt, P., Verhaegen, F. & Messens, K. (1998) Heterogeneous photobleaching in confocal microscopy caused by differences in refractive index and excitation mode. *Cytometry* **32**, 137–146.

Vermolen, B. J., Garini, Y., Mai, S., *et al.* (2005) Characterizing the three-dimensional organization of telomeres. *Cytometry A* **67**(2), 144–150.

Wilson, T. (1995) The role of the pinhole in confocal imaging system. *Handbook of Biological Confocal Microscopy* 2nd ed. (ed. by J. Pawley) pp. 167–182. Springer, New York, NY.

Wilson B. C., Patterson M. S. & Lilge L. (1997) Implicit and explicit dosimetry in photodynamic therapy: a new paradigm lasers in medicine **12**(3), 182–199

Young, I. T. (1996) Quantitative microscopy. *IEEE Eng. Med. Biol.* **15**(1), 59–66.

Young, I. T., Garini, Y., Vermolen, B., *et al.* (2006) Absolute fluorescence calibration. *Proc. SPIE*. 6088, 1–9.

Zucker, R. M. (2006a) Evaluation of confocal microscopy system performance. *Methods Mol. Biol.* **319**, 77–135.

Zucker, R. M. (2006b) Quality assessment of confocal microscopy slide-based systems: instability. *Cytometry A* **69A**(7), 677–690.

Zucker, R. M. & Price, O. (2001a) Evaluation of confocal microscopy system performance. *Cytometry A* **44**(4), 273–294.

Zucker, R. M. & Price, O. T. (2001b) Statistical evaluation of confocal microscopy images. *Cytometry A* **44**(4), 295–308.

Zwier J. M., Brakenhoff G. J., Savenije M., Pasierbek P. & Paiha K. (2006) Sectioning imaging property (SIP) charts a tool for characterisation of confocal fluorescence microscope systems. *Microsc. Imaging* **8**(2), 54–57.

Zwier, J. M., Oomen, L., Brocks, L., Jalink, K. & Brakenhoff, G. J. (2008) Quantitative image correction and calibration for confocal fluorescence microscopy using thin reference layers and SIPchart-based calibration procedures. *J. Microsc.* **216**(1), 15–24.

Zwier, J.M., van Rooij, G.J., Hofstraat, J.W., Brakenhoff, G.J. (2004) Image calibration in fluorescence microscopy. *J. Microsc.* **231**(1): 59–69.